Journal of Solid State Chemistry **162,** 182–187 (2001)
doi:10.1006/jssc.2001.9223, available online at http://www.idealibrary.com on IDEAL®

Crystal Structure and Magnetic Properties of a New Oxyselenide of Gadolinium and Titanium: $Gd_4TiSe_4O_4$

A. Meerschaut,[1] A. Lafond, V. Meignen, and C. Deudon

Institut des Matériaux Jean Rouxel, UMR 6502 CNRS—Université de Nantes, Laboratoire de Chimie des Solides, 2, rue de la Houssinière, BP 32229, 44322 Nantes cedex 03, France

Received January 23, 2001; in revised form April 11, 2001; accepted April 20, 2001; published online June 1, 2001

IN HONOR OF PROFESSOR PAUL HAGENMULLER ON THE OCCASION OF HIS 80TH BIRTHDAY

A new compound $Gd_4TiSe_4O_4$ has been obtained by a solid state reaction of Gd_2O_3, TiO_2, and $TiSe_2$, at $T = 1000°C$, with the addition of iodine to favor crystallization. Single-crystal X-ray diffraction measurements show that $Gd_4TiSe_4O_4$ crystallizes in space group $C2/m$ (No. 12) of the monoclinic system with two formula units in a cell of dimensions $a = 15.7878(4)$ Å, $b = 3.7610(2)$ Å, $c = 9.6639(3)$ Å, and $\beta = 117.569(2)°$. The structure contains two crystallographically independent Gd atoms with a bicapped trigonal prismatic coordination. Association of four adjacent Gd-centered polyhedra constitutes the elemental building unit, which develops into ribbons along b. The ribbons are interconnected by infinite chains of edge-sharing Ti-centered octahedra. Magnetic susceptibility of the title compound has been measured from 1.8 to 300 K, and from $B = 1.10^{-3}$ to 0.1 T for the ZFC and FC cooling modes. The linear variation of the inverse susceptibility versus T can be modeled with a Curie–Weiss law in agreement with a Gd^{3+} free ion behavior. The maximum of the χ(T) curve at about 2.5 K could be attributed to both an antiferromagnetic transition and the saturation of the weak ferromagnetic component. © 2001 Elsevier Science

Key Words: **gadolinium; titanium; oxyselenide; crystal structure; magnetism.**

INTRODUCTION

Most of the discoveries of binary compounds in the rare earth–chalcogen system were made in the 1960s; this concerned for instance the Ln_2X_3 series. Just after, searches on $LnLn'X_3$ and $LnTX_3$ (T = transition metal) were undertaken. In this field, a great scientific contribution was supplied by Flahaut and his coworkers (see for instance the review article written by Flahaut in 1979 (1)). In this article, mention of ternary compounds with a rare earth metal and two kinds of anions, namely oxygen and chalcogen, was also made. A few years later, a new family of quaternary compounds with two metal atoms (rare earth and post transition metal) and two types of anions (oxygen and chalcogen (X = S, Se)) was reported by the same team (2). These oxychalcogenides formed by a rare earth element and a second metal crystallize in a layered type structure, with a composite character owing to the alternation of an oxide sheet [LnO] and a sulfide sheet [T_xX_y]. Two very recent papers (3, 4) reported the existence of a new family of quaternary compounds with rare earth and titanium as metals, and with oxygen and sulfur as anions, for which a composite layered approach was also put forward. Indeed, these phases formulated as $Ln_2Ti_2S_2O_5$ can be very schematically described as an alternation of slabs of different chemical nature, with this time a sulfide slab [Ln_2S_2] and an oxide slab [Ti_2O_5]. In order to enlarge this last family, we tried to synthesize the corresponding selenide derivatives. For the corresponding samarium compound, attempts to get $Sm_2Ti_2Se_2O_5$ have failed, but the presence of a new compound $Sm_3Ti_3Se_2O_8$, in a very small amount, was detected (5). Although the initial ratios between starting components for the gadolinium batch were identical to that of the samarium batch (the objective being $Ln_2Ti_2Se_2O_5$), we found very few dark gray crystals in a needle shape, whose chemical analysis revealed the approximate $Gd_4TiSe_4O_4$ composition. We present, here, the synthesis, crystal structure, and magnetic properties of this new phase.

SYNTHESIS AND CHEMICAL ANALYSIS

$Gd_4TiSe_4O_4$ was obtained from the reaction of Gd_2O_3, TiO_2, and $TiSe_2$, in the ratio 1 : 1 : 1, which would have led to the $Gd_2Ti_2Se_2O_5$ composition. The initial mixture was heated at 1000°C during one week, with an intermediate grinding as well as addition of iodine to favor crystallization. A very small amount of dark gray single crystals, in a ribbon-like or needle shape was identified among the

[1]To whom correspondence should be addressed. Fax: (33) 2 40 37 39 95. E-mail: meerschaut@cnrs-imn.fr.

0022-4596/01 $35.00

reaction product mainly constituted by $TiSe_2$ and $Gd_2Ti_2O_7$ phases. Chemical analysis of this synthetic compound (glued in epoxy (araldite) and then polished) using an EDS-equipped scanning electron microscope gave the following atomic percentages: Gd 30.0 (1.8)%, Ti 7.1 (0.3)%, Se 28.6 (1.1)%, and O 33.6 (1.0)%; the values (atomic percentages) deduced from the X-ray structure determination are 30.8, 7.7, 30.8, and 30.8%, respectively. Oxygen content is by no means reliable (too overestimated), while a slight deficit in Ti and Se is noticed. Traces of iodine were detected (0.7 (0.6)%); the question of its nature, intrinsic or extrinsic (surface contamination) is not solved.

STRUCTURE DETERMINATION

A single crystal in a needle shape, of dimensions $0.012 \times 0.018 \times 0.32\ mm^3$, was mounted on a STOE-IPDS single φ axis diffractometer with a 2D area detector based on Imaging Plate technology. The crystal-to-detector distance was set to 70 mm, which means a 2θ range between 3.3° and 52.1°. Operating conditions and X-ray crystallographic details are given in Table 1. Two hundred exposures were processed using the STOE software. Cell parameters calculated from 1937 saved peaks gave, in the nonconventional monoclinic *I*-centered symmetry, the following values: $a = 9.662(2)$ Å, $b = 3.7563(8)$ Å, $c = 14.186(2)$ Å, and $\beta = 99.49(2)°$.

Transformation from the original cell using the $[101, 010, \bar{1}00]$ matrix leads to the conventional C-centered monoclinic symmetry with unit cell parameters: $a = 15.792(3)$ Å, $b = 3.7563(8)$ Å, $c = 9.662(2)$ Å, and $\beta = 117.63(3)°$.

An X-ray powder pattern was recorded on a SIEMENS diffractometer with Bragg–Brentano geometry from ground-selected crystals, crushed on the sample holder, which could favor a strong preferential orientation. Cell parameters were determined from a full pattern matching refinement using the FULLPROF program (6). One can notice, in Fig. 1, the presence of a small amount of parasitic phases, $Gd_2Ti_2O_7$ and $TiSe_2$ ($\approx 5\%$). This yields to cell parameter values: $a = 15.7878(4)$ Å, $b = 3.7610(2)$ Å, $c = 9.6639(3)$ Å, and $\beta = 117.569(2)°$, in good agreement with the previous values.

The crystal structure of $Gd_4TiSe_4O_4$ was solved by means of direct methods and subsequent difference-Fourier syntheses (SHELXTL program (7)) in the space group $C2/m$. An absorption correction, calculated from the face-indexed option by Gaussian integration method, was applied. Isotropic refinement, using the JANA98 suite of programs (8), gave $R_F = 5.73\%$, and anisotropic refinements of all atoms except oxygen converged to a reliability factor $R_F = 3.88\%$, and $R_W = 4.68\%$, for 466 reflections satisfying the criterion $I \geq 3\sigma(I)$ and 36 parameters. Fractional coordinates and equivalent atomic displacement parameters (isotropic for O) are compiled in Table 2; anisotropic displacement parameters for Gd, Se, and Ti atoms are given in Table 3. The U_{22} of Ti was much higher than those of the other atoms,

TABLE 1
Cell Parameters, Crystallographic Data, Refinement Results for $Gd_4TiSe_4O_4$

Physical and crystallographic data	
Formula	$Gd_4Ti_1Se_4O_4$
Molar mass (g/mol^{-1})	1056.7
Color	Dark gray
crystal size (mm^3)	$0.012 \times 0.32 \times 0.018$
boundaries	{(100}, {010}, {001}
Space group	$C2/m$ (No. 12)
Z	2
a(Å)	15.7878(4)
b(Å)	3.7610(2)
c(Å)	9.6639(3)
β	117.569(2)
V(Å^3)	508.67(4)
Calculated density (g/cm^{-3})	6.90
Absorption coefficient (mm^{-1})	40.75
Recording conditions	
Temperature (K)	293
Radiation λ (Å)	0.71073 (Mo$K\alpha$)
Diffractometer	STOE Image plate
Angular range θ (°)	2.24–25.74
$-h, +h; -k, +k; -l, +l$ range	−18, 18; −4, 4; −11, 11
Data reduction	
Recorded reflections all; obs ($I > 2\sigma(I)$)	1937; 1538
Independent reflections all; obs ($I > 3\sigma(I)$)	543; 466
Absorption correction	Gaussian method based on crystal shape
Transmission min–max	0.388–0.633
Refinement	
No. of refined parameters	36
R_F/R_w(%) on obs. reflections ($I \div 3\sigma(I)$)	3.88/4.68
R_F/R_w (%) on all reflections	4.47/4.70
Goodness of fit	3.39
Isotropic extinction (type I)	0.18(2)
Residual electronic density e^-/Å^3 (deapest/highest)	−3.30; +5.66

TABLE 2
Atomic Positions and Isotropic/Equivalent Atomic Displacement Parameters for $Gd_4TiSe_4O_4$

Atom	Site	s.o.f.	x	y	z	U_{iso}/U^*_{eq}
Gd1	4*i*	1	0.47535(3)	0	0.66922(5)	0.0046(2)*
Gd2	4*i*	1	0.27623(4)	$-\frac{1}{2}$	0.67520(5)	0.0061(2)*
Se1	4*i*	1	0.62365(8)	0	0.0160(1)	0.0106(4)*
Se2	4*i*	1	0.61553(7)	$\frac{1}{2}$	0.6318(1)	0.0083(4)*
Ti	2*a*	1	0	0	0	0.024(1)*
O1	4*i*	1	0.4490(5)	$\frac{1}{2}$	0.7801(8)	0.005(1)
O2	4*i*	1	0.3163(5)	0	0.5913(8)	0.005(1)

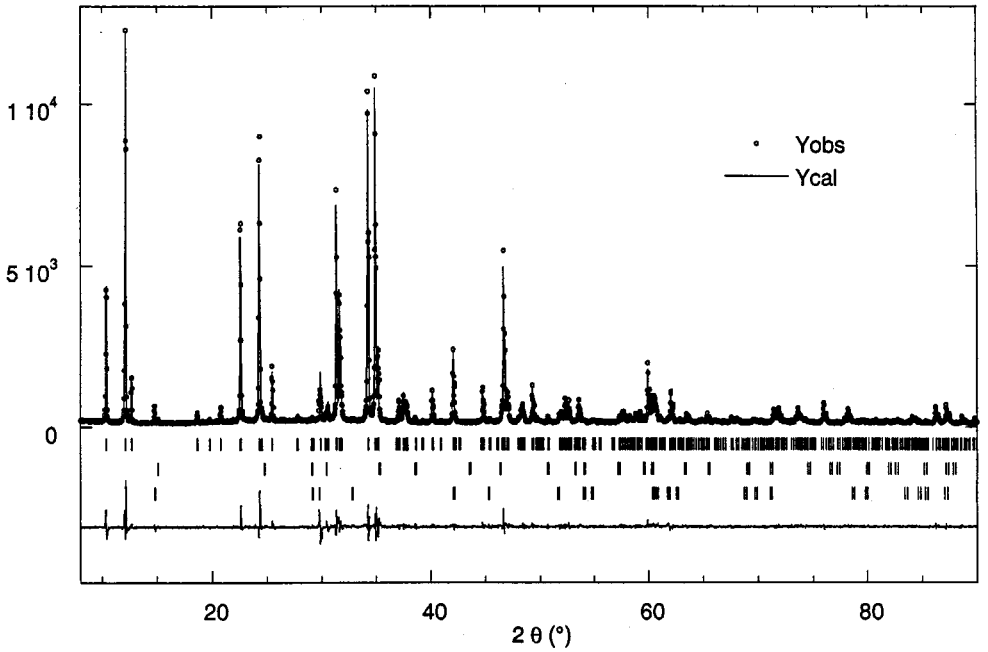

FIG. 1. Observed and calculated X-ray pattern for $Gd_4TiSe_4O_4$, $Gd_2Ti_2O_7$, and $TiSe_2$. The ticks indicate the series of Bragg positions of these three phases, from the top to the bottom, respectively.

while in the same time U_{33} is too low, indicating perhaps a less symmetrical position [4*g* $(0, y, 0)$ with y close to 0, instead of the special 2*a* site $(0,0,0)$], in a statistical occupancy (50%). This situation was frequently observed for Ti-coordination in some parent compounds as exemplified by $La_4Ti_3S_4O_8$ (9), and $La_8Ti_{10}S_{24}O_4$ (10, 11), to achieve a "distorted octahedral" coordination (close to a tetrahedral coordination). Refinement of this hypothesis, but isotropic for Ti because of instability (divergence!) led to a value $y = 0.045$, with a slightly higher R factor ($R_F = 4.05\%$, $U_{iso}(Ti) = 0.013$ Å^2). However, whatever the solution for Ti (i.e., site 2*a* or site 4*g* (split position—statistic)), the final difference-Fourier always indicated a highest residual peak (~ 5.7 e$^-$/Å^3), at coordinates (ca. 0.67, 0., 0.01), close to Se1 (~ 0.8 Å). The question of a very slight selenium to iodine substitution is open. Such a possibility was tested through a fixed Se/I content, precisely 95%/5%, respectively. No significant improvement was achieved, apart from a lesser importance of the residuals. This model was not kept because the presence of iodine remains questionable.

TABLE 3
Anisotropic Atomic Displacement Parameters of $Gd_4TiSe_4O_4$

	U_{11}	U_{22}	U_{33}	U_{12}	U_{13}	U_{23}
Gd1	0.0052(3)	0.0044(4)	0.0031(3)	0	0.0009(2)	0
Gd2	0.0073(3)	0.0045(4)	0.0026(3)	0	−0.0010(2)	0
Se1	0.0147(5)	0.0085(7)	0.0020(5)	0	−0.0018(4)	0
Se2	0.0076(5)	0.0076(7)	0.0076(5)	0	0.0016(4)	0
Ti	0.021(2)	0.045(3)	0.0002(10)	0	0.000(1)	0

DESCRIPTION OF THE CRYSTAL STRUCTURE

The crystal structure viewed down the unique axis *b* is shown in Fig. 2. Gadolinium and titanium atoms are well distinguished by their different coordination polyhedra,

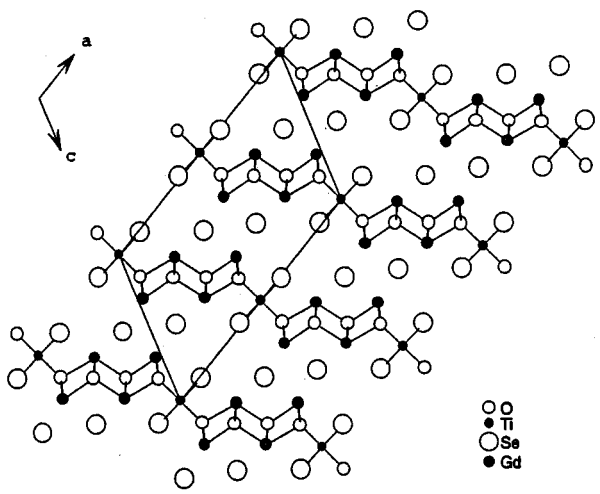

FIG. 2. Projection of the structure of $Gd_4TiSe_4O_4$ along the *b* axis.

TABLE 4
Interatomic Distances and Bond Valences for $Gd_4TiSe_4O_4$

Atom 1	Atom 2	Sym. op.	Distance (Å)	Bond val.	Atom 1	Atom 2	Sym. op.	Distance (Å)	Bond val.
Gd1	1 × Se1	**2**	3.074(1)	0.318	Ti	4 × Se1	**7; 8; 12; 13**	2.6632(9)	0.465
Gd1	2 × Se2	**1; 3**	3.051(1)	0.338	Ti	2 × O1	**9; 14**	1.892(7)	0.812
									Σ = 3.485
Gd1	2 × Se2	**4; 5**	3.1926(9)	0.231					
Gd1	2 × O1	**1; 3**	2.296(5)	0.536					
Gd1	1 × O2	**1**	2.263(7)	0.586					
				Σ = 3.113					
Gd2	2 × Se1	**4; 6**	3.2520(9)	0.197					
Gd2	2 × Se2	**11; 13**	3.027(1)	0.361					
Gd2	1 × O1	**3**	2.430(7)	0.373					
Gd2	2 × O2	**1; 3**	2.251(5)	0.605					
Gd2	1 × O2	**10**	2.299(6)	0.531					
				Σ = 3.229					

Note. 1: x, y, z; **2**: $x, y, 1+z$; **3**: $x, -1+y, z$; **4**: $1-x, -y, 1-z$; **5**: $1-x, 1-y, 1-z$; **6**: $1-x, -1-y, 1-z$; **7**: $\frac{1}{2}-x, \frac{1}{2}-y, -z$; **8**: $\frac{1}{2}-x, -\frac{1}{2}-y, -z$; **9**: $\frac{1}{2}-x, \frac{1}{2}-y, 1-z$; **10**: $\frac{1}{2}-x, -\frac{1}{2}-y, 1-z$; **11**: $-\frac{1}{2}+x, -\frac{3}{2}+y, z$; **12**: $-\frac{1}{2}+x, \frac{1}{2}+y, z$; **13**: $-\frac{1}{2}+x, -\frac{1}{2}+y, z$; **14**: $-\frac{1}{2}+x, -\frac{1}{2}+y, -1+z$.

namely a bicapped trigonal prismatic type and an octahedral type, respectively. Table 4 summarizes the main interatomic distances within each centered metal atom polyhedron. Such a segregation of metal polyhedra is well known in *Ln*–Ti oxychalcogenide compounds, as illustrated for instance in the three new compounds $Ln_{3.67}Ti_2Se_6O_3$ (*Ln* = Ce, Nd, Sm), very recently reported (12). The Ti atom is octahedrally coordinated by 4 Se1 and 2 apical O1 atoms. Gd1 and Gd2 are both found in bicapped trigonal prisms. Gd1 is surrounded by 5 Se and 3 O atoms, the two capping atoms being 1 Se and 1 O, while Gd2 is coordinated by 4 Se and 4 O atoms, the two capping atoms being O atoms (see Fig. 3). Association of 4 adjacent Gd-polyhedra (Gd1 and Gd2 centered) (see Fig. 3) constitutes the elemental building unit, which develops into ribbons along *b*.

These ribbons are interconnected by infinite chains of edge-sharing (Se1–Se1) Ti-centered octahedra. Figure 4 illustrates the situation corresponding to the split position for Ti (4*g* site).

The structure of $Gd_4TiSe_4O_4$ can be considered as resulting from the intergrowth of serrated [GdO] slabs connected by titanium atoms, and serrated sheets of Se atoms. Such a structural model could recall the model proposed for the structure of $(LaO)_4Se_3$ (13). In that way, the structure of $(LaO)_4Se_3$ is relevant to the stacking of regular [LaO] slabs interleaved by planar Se sheets, along the *a*-direction (see Fig. 5). But in $(LaO)_4Se_3$, association of La-polyhedra, giving rise to a regular plane, is not interrupted by the presence of Ti octahedra, contrary to $Gd_4TiSe_4O_4$.

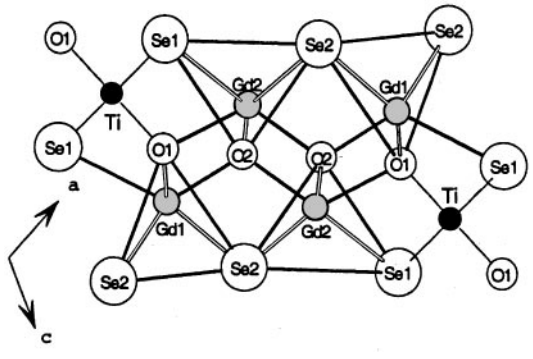

FIG. 3. View of the elemental building block of the compound $Gd_4TiSe_4O_4$ showing the connectivity between bicapped trigonal prisms around Gd atoms.

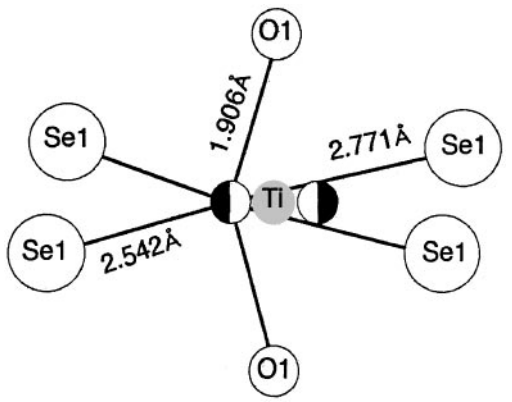

FIG. 4. Detailed environment around titanium showing the split position of this atom (0, ± 0.043, 0).

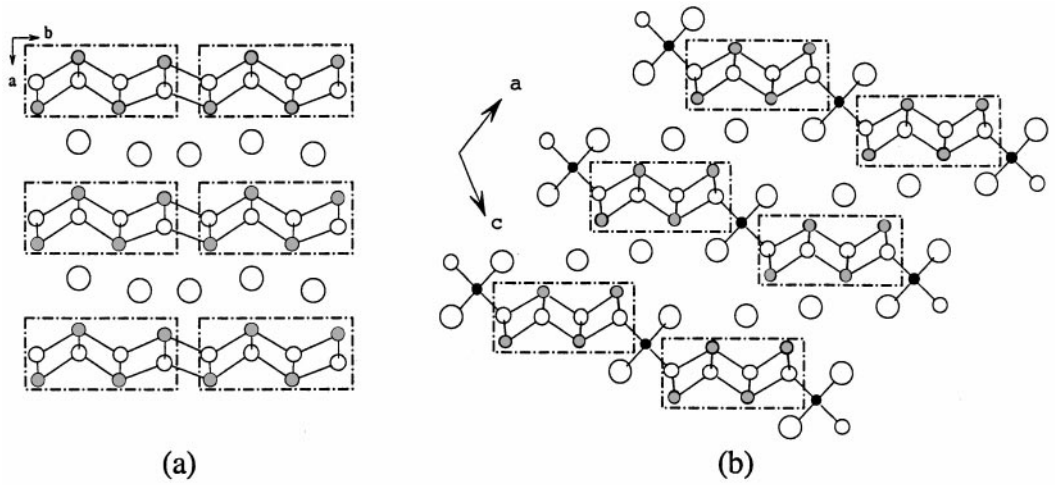

FIG. 5. (a) Projection of the structure of $(LaO)_4Se_3$ onto the (a, b) plane showing the intergrowth of [LaO] planes and serrated sheets of Se atoms; (b) for comparison, drawing of the alternated stacking sequence of [GdO] and [Se] units for$Gd_4TiSe_4O_4$.

Bond Valence Calculations

The charge balance is achieved in the phase $Gd_4TiSe_4O_4$ with Gd(+ III) and Ti(+ IV) against Se(− II) and O(− II). Bond valence calculations using the expression $v_{ij} = \exp[(R_{ij} - d_{ij})/b]$ (where $b = 0.37$ and $R_0(\text{Ti(IV)}) = 1.815$ Å, $R_0(\text{Ti–Se}) = 2.38$ Å, and d_{ij} are the experimental interatomic distances [14]) agree with the Gd(+ III) oxidation state, but rather differ with the Ti(+ IV) (see Table 4).

MAGNETIC MEASUREMENTS

Magnetic dc susceptibility ($\chi_{dc} = \mu_o M^t/B$) has been measured in the 1.8–300 K temperature range and from $B = 1 \times 10^{-3}$ to 0.1 T for the ZFC and FC cooling modes. The low temperature isothermal magnetic moment has been measured in the 1×10^{-3}–1 T field range. These measurements were performed on the sample analyzed by X-ray diffraction technique ($m \approx 6$ mg). Raw data were corrected for the sample holder contribution (< 5%) and for the diamagnetic core-electron contribution according to the Pascal's constants ($\chi_{dia} = -3.4.10^{-4}$ emu/mol $= -4.5 \times 10^{-9}$ m^3/mol).

There is no difference between the ZFC and FC data. The linear variation of the inverse susceptibility versus temperature can be modeled by a Curie–Weiss law ($\chi = C/(T - \theta_p)$). In the 30–300 K temperature range, these data lead to $C = 7.52(1)$ emu K mol$^{-1} = 9.45(1) \times 10^{-5}$ m^{3}K mol^{-1} and $\theta_p = -12.8(2)$ K. The negative value of the paramagnetic temperature indicates that antiferromagnetic interactions could occur in this compound. The effective moment deduced from the Curie constant ($\mu_{eff} = 7.75\ \mu_B$/Gd) is close to the Landé value for Gd^{3+} ($\mu_{th} = 7.94\ \mu_B$/Gd). This result agrees with the + IV oxidation state for Ti as deduced from the charge balance in $Gd_4TiSe_4O_4$.

The low-temperature susceptibility shows a drastic increase between 4 and 2.5 K and then a sharp decrease below 2.5 K (see Fig. 6). Let us examine if this unconventional behavior could be due to the presence of impurities. The sample used for these magnetic measurements was a collection of small selected crystals. X-ray powder analysis shows the presence of a small amount of two additional phases: $TiSe_2$ and $Gd_2Ti_2O_7$. An old report for $Gd_2Ti_2O_7$ indicated that no long-range order takes place down to 1 K (15). A recent work on this compound indicates that the

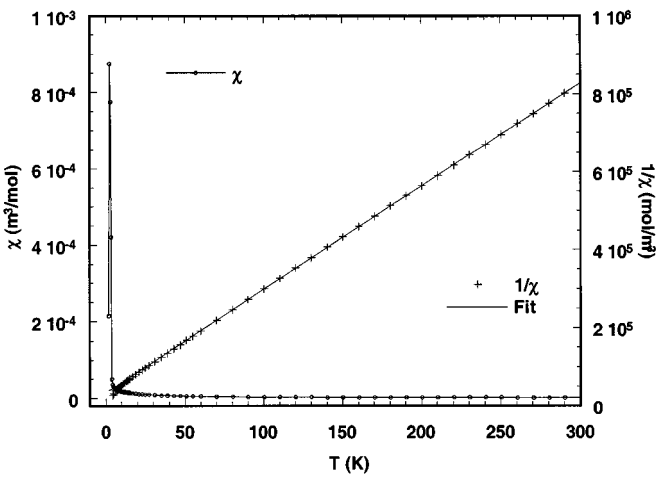

FIG. 6. Magnetic susceptibility and inverse susceptibility of $Gd_4TiSe_4O_4$ versus temperature under 0.01 T. One can notice a very sharp peak at about 2.5 K. The Curie–Weiss fit leads to $C = 7.52(1)$ emu K/mol$^{-1} = 9.45(1) \times 10^{-5}$ m^3 K mol^{-1} and $\theta_p = -12.8(2)$ K.

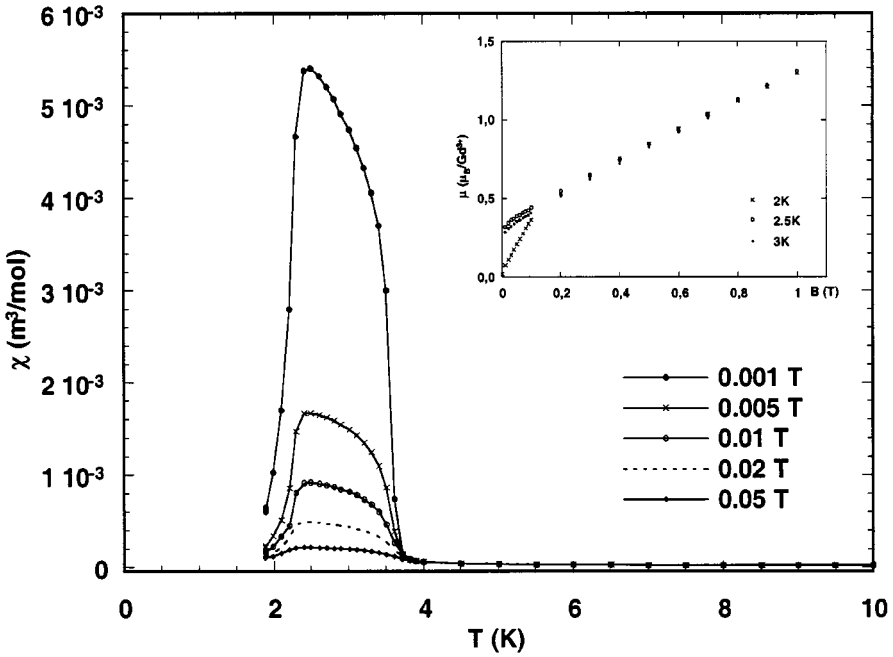

FIG. 7. Field dependence of the magnetic susceptibility at low temperature. The inset shows the magnetization curves versus the applied field for 2, 2.5, and 3 K.

deviation from a Curie–Weiss law below 10 K is due to the frustrated antiferromagnetic interactions between Gd^{3+} cations (16). Thus the sharp maximum observed for our sample cannot be attributed to the presence of $Gd_2Ti_2O_7$ and seems to be an intrinsic behavior of the title compound. This maximum is too sharp to be attributed to an antiferromagnetic transition alone. In addition, the susceptibility is highly field-dependent in this temperature range (see Fig. 7). The field dependence of the magnetic moment (per 1 formula unit) is shown on the inset of Fig. 7 for 2, 2.5, and 3 K. One can see a ferromagnetic component which saturates at very low field (≈ 0.01 T) at 2.5 and 3 K. This behavior agrees with the field dependence of the susceptibility. By extrapolation of the linear part of the $M^t(B)$ curves down to $B = 0$, one can deduce a ferromagnetic component of about 0.36 μ_B/Gd^{3+}. This component corresponds to 5% of the saturated magnetic moment (7 μ_B/Gd^{3+}) and could be attributed to a small canting ($\approx 3^\circ$) of the magnetic moments. This canting disappears below 2.5 K where the material gives rise to a collinear antiferromagnetic long-range order. The maximum of the $\chi(T)$ curve is due to both the antiferromagnetic transition and the saturation of the weak ferromagnetic component. This magnetic model cannot be checked by means of neutron diffraction because gadolinium is a huge neutron absorber (absorption cross section $\sigma_a = 49700$ barn). The preparation of the terbium homologue, which is suitable for neutron studies ($\sigma_a = 23.4$ barn), is in progress.

REFERENCES

1. J. Flahaut, *In* "Handbook on the Physics and Chemistry of Rare Earths" (K. A. Gschneider, Jr. and L. Eyring, Eds.). North Holland, Amsterdam, 1979.
2. M. Guittard, S. Benazeth, J. Dugué, S. Jaulmes, M. Palazzi, P. Laruelle, and J. Flahaut, *J. Solid State Chem.* **51,** 227–238 (1984).
3. C. Boyer, C. Deudon, and A. Meerschaut, *C. R. Acad. Sci. Paris Sér. IIc* 93–99 (1999).
4. M. Goga, R. Seshadri, V. Ksenofontov, P. Gütlich, and W. Tremel, *J. Chem. Soc., Chem. Commun.* 979–980 (1999).
5. V. Meignen, C. Deudon, A. Lafond, C. Boyer-Candalen, and A. Meerschaut, *Solid State Sciences* **3,** 189–194 (2001).
6. J. Rodriguez-Carvajal, "FULLPROF version 3.5d: Program for Rietveld Refinement and Pattern Matching Analysis," France, 1998.
7. G. M. Sheldrick, "SHELXL-97," Crystal Structure Refinement, UNIX version, Release 97-2, 1997.
8. V. Petricek and M. Dusek, "JANA98: Crystallographic Computing System." Institute of Physics, Academy of Sciences of the Czech Republic, Praha, 1998.
9. J. A. Cody and J. A. Ibers, *J. Solid State Chem.* **114,** 406–412 (1995).
10. L. Cario, C. Deudon, A. Meerschaut, and J. Rouxel, *J. Solid State Chem.* **136,** 46–50 (1998).
11. L. J. Tranchitella, J. C. Fettinger, S. F. Heller-Zeisler, and B. W. Eichhorn, *Chem. Mater.* **10,** 2078–2085 (1998).
12. O. Tougait and J. A. Ibers, *Chem. Mater.* **12,** 2653–2658 (2000).
13. J. Dugué, C. Adolphe, and P. Khodadad, *Acta Crystallogr. Sect. B* **26,** 1627–1628 (1970).
14. N. E. Brese and M. O'Keefe, *Acta Crystallogr. Sect. B* **47,** 192–197 (1991).
15. J. D. Cashion, A. H. Cooke, M. J. M. Leask, T. L. Thorp, and M. R. Wells, *J. Mater. Sci.* **3,** 402 (1968).
16. N. P. Raju, M. Dion, M. J. P. Gingras, T. E. Mason, and J. E. Greedan, *Phys. Rev. B.* **59**(22), 14489 (1999).